DOI: 10.1021/ic902131a

Inorganic Chemistry
Article

Ultrathin SnO_2 Nanorods: Template- and Surfactant-Free Solution Phase Synthesis, Growth Mechanism, Optical, Gas-Sensing, and Surface Adsorption Properties

Guangcheng Xi and Jinhua Ye*

International Center for Materials Nanoarchitectonic, and Photocatalytic Materials Center, National Institute for Materials Science, 1-2-1 Sengen, Tsukuba, Ibaraki 305-0047, Japan

Received October 27, 2009

A novel template- and surfactant-free low temperature solution-phase method has been successfully developed for the controlled synthesis of ultrathin SnO_2 single-crystalline nanorods for the first time. The ultrathin SnO_2 single-crystalline nanorods are 2.0 ± 0.5 nm in diameter, which is smaller than its exciton Bohr radius. The ultrathin SnO_2 nanorods show a high specific area (191.5 $m^2\ g^{-1}$). Such a thin SnO_2 single-crystalline nanorod is new in the family of SnO_2 nanostrucures and presents a strong quantum confinement effect. Its formation depends on the reaction temperature as well as on the concentration of the urea solution. A nonclassical crystallization process, Ostwald ripening process followed by an oriented attachment mechanism, is proposed based on the detailed observations from a time-dependent crystal evolution process. Importantly, such structured SnO_2 has shown a strong structure-induced enhancement of gas-sensing properties and has exhibited greatly enhanced gas-sensing property for the detection of ethanol than that of other structured SnO_2, such as the powders of nanobelts and microrods. Moreover, these ultrathin SnO_2 nanorods exhibit excellent ability to remove organic pollutant in wastewater by enormous surface adsorption. These properties are mainly attributed to its higher surface-to-volume ratio and ultrathin diameter. This work provides a novel low temperature, green, and inexpensive pathway to the synthesis of ultrathin nanorods, offering a new material form for sensors, solar cells, catalysts, water treatments, and other applications.

Introduction

Semiconducting metal oxide nanocrystals have a wide range of applications in photocatalysts, battery materials, sensors, and optoelectronic devices because of their quantum confinement effect and size- and shape-dependent characteristics.[1−4] In particular, SnO_2 nanocrystals are important owing to their potential applications based on gas sensing,[5,6] field-emission,[7] electrochemical[8] and photocatalytic properties.[9] Recently, these useful properties have stimulated the search for new synthetic methodologies for well-controlled SnO_2 nanostructures. Several reports on high-temperature physical SnO_2 syntheses have been published.[10] Compared with high-temperature physical synthetic methods, the chemical methods appear to be of particular interest because they offer the potential of facile scale-up and occur at moderate temperatures. The chemical syntheses of SnO_2 nanostructures are generally carried out in water or high boiling point organic solvent using tin salts or organic tin as starting materials in the presence of surfactants.[11] These

*To whom correspondence should be addressed. E-mail: jinhua.ye@nims.go.jp. Phone: +81 29 859 2646. Fax: +81 29 859 2301.

(1) Wang, Z. L.; Song, J. H. *Science* **2006**, *312*, 242.
(2) (a) Tang, Z. Y.; Zhang, Z. L.; Wang, Y.; Glotzer, S. C.; Kotov, N. A. *Science* **2006**, *314*, 274. (b) Tang, Z. Y.; Wang, Y.; Shanbhag, S.; Kotov, N. A. *J. Am. Chem. Soc.* **2006**, *128*, 7036. (c) Tang, Z. Y.; Wang, Y.; Shanbhag, S.; Giersig, M.; Kotov, N. A. *J. Am. Chem. Soc.* **2006**, *128*, 6730.
(3) Zhan, J. H.; Bando, Y.; Hu, J. Q.; Xu, F. F.; Golberg, D. *Small* **2005**, *1*, 883.
(4) Sun, X. M.; Li, Y. D. *Angew. Chem., Int. Ed.* **2004**, *43*, 3827.
(5) (a) Liu, Z.; Zhang, D.; Han, S.; Li, C.; Tang, T.; Jin, W.; Liu, X.; Zhou, C. *Adv. Mater.* **2003**, *15*, 1754. (b) Epifani, M.; Diaz, R.; Arbiol, J.; Comini, E.; Sergent, N.; Pagnier, T.; Siciliano, P.; Faglia, G.; Morante, J. R. *Adv. Funct. Mater.* **2006**, *16*, 1488.
(6) Kolmakov, A.; Klenov, D. O.; Lilach, Y.; Stemmer, S.; Moskovits, M. *Nano Lett.* **2005**, *5*, 667.
(7) He, J. H.; Wu, T. H.; Hsin, C. L.; Li, K. M.; Chen, L. J.; Chueh, Y. L.; Chou, L. J.; Wang, Z. L. *Small* **2006**, *2*, 116.
(8) (a) Wen, Z. H.; Wang, Q.; Zhang, Q.; Li, J. H. *Adv. Funct. Mater.* **2007**, *17*, 2772. (b) Lee, K. T.; Lytle, J.; Ergang, N. S.; Oh, S.; Stein, A. *Adv. Funct. Mater.* **2005**, *15*, 547.
(9) Wang, W. W.; Zhu, Y. J.; Yang, L. X. *Adv. Funct. Mater.* **2007**, *17*, 50.
(10) (a) Pan, Z. W.; Dai, Z. R.; Wang, Z. L. *Science* **2001**, *291*, 1947. (b) Hu, J.; Bando, Y.; Liu, Q.; Golberg, D. *Adv. Funct. Mater.* **2003**, *13*, 493. (c) Mathur, S.; Barth, S. *Small* **2007**, *3*, 2070. (d) Liu, Y.; Dong, J.; Liu, M. *Adv. Mater.* **2004**, *16*, 353. (e) Duan, J. H.; Yang, S. G.; Liu, H. W.; Gong, J.; Huang, H. B.; Zhao, X. N.; Zhang, R.; Du, Y. W. *J. Am. Chem. Soc.* **2005**, *127*, 6180. (f) Yang, R.; Wang, Z. L. *J. Am. Chem. Soc.* **2006**, *128*, 1466.
(11) (a) Ba, J. H.; Polleux, J.; Antonietti, M.; Niederberger, M. *Adv. Mater.* **2005**, *17*, 2509. (b) Lou, X. W.; Yuan, C.; Archer, L. A. *Small* **2007**, *2*, 261. (c) Vayssieres, L.; Graetzel, M. *Angew. Chem., Int. Ed.* **2004**, *43*, 3666. (d) Baumann, T. F.; Kucheyev, S. O.; Gash, A. E.; Satcher, J. H. *Adv. Mater.* **2005**, *17*, 1546.

Published on Web 01/20/2010

methods are convenient and may lead to SnO_2 nanomaterials of controlled morphology. For example, using oleylamine as solvent and oleic acid as surfactant, Li and co-workers synthesized SnO_2 single-crystalline nanorods with a diameter of about 5 nm based on the oleylamine-assisted hydrolysis of tin alkoxide in the presence of high content of oleic acid at 180 °C.[12] Wang and co-workers demonstrated the synthesis of twisted and branched SnO_2 poly crystalline nanowires with diameters of 1.5−4.5 nm by a solvothermal process at 180 °C, combined with the introduction of oleylamine and oleic acid used as surfactants.[13]

It is well-known now that the size and morphology of the nanomaterials greatly affect their properties as well their further applications. Particularly for SnO_2 nanomaterials, early studies demonstrated that their gas sensing performance is affected by several structural parameters such as particle size, surface-to-volume ratio, and crystallinity.[14] For example, small particle size, a large surface-volume ratio, and high crystallinity are required to enhance the sensitivity of gas sensors. Although many one-dimensional (1-D) SnO_2 nanostructures have been synthesized by chemical methods, such as solution-phase precursor route,[15] microemulsions,[16] template methods,[17] and hydrothermal methods,[18] most of these 1-D SnO_2 nanocrystals have diameters larger than that required for the emergence of the quantum confinement effect (the exciton Bohr radius of SnO_2 is only 2.7 nm). This limits their applications, to some extent. Recently, Samulski and co-workers have demonstrated the synthesis of SnO_2 single-crystalline nanorods with a diameter of 3.4 nm by a hydrothermal process at 150 °C.[19] However, the development of template- and surfactant-free low temperature routes (<100 °C) for the production of ultrathin SnO_2 single-crystalline nanorods remains a challenge.

In the present work, we demonstrate a facile and economical route for the large-scale synthesis of ultrathin SnO_2 single-crystalline nanorods with an average diameter of 2 ± 0.5 nm via a simple hydrolysis reaction of tin tetrachloride with urea at 90 °C, using neither template nor surfactant. Briefly, $SnCl_4$ is mixed with $CO(NH_2)_2$ in aqueous solution at room temperature and atmospheric pressure, and the mixture is then heated at 90 °C for 24 h, which permits ultrathin SnO_2 single-crystalline nanorods to form. Experimental observations suggest SnO_2 nanorods are formed by a nonclassical crystallization process: classical Ostwald ripening process followed by a nonclassical oriented attachment mechanism. Furthermore, these ultrathin SnO_2 nanorods exhibit enhanced gas-sensing activity and excellent ability to remove organic pollutant in wastewater.

Experimental Section

Chemicals. Five hydrated tin tetrachloride ($SnCl_4 \cdot 5H_2O$), urea ($CO(NH_2)_2$,), fuming hydrochloride (HCl, 37%), superpure water (Millipore, 18.2 MΩcm), absolute ethanol. All reagents used were analytically pure, and were purchased from Beijing Chemical Reagent Company and were used without further purification.

Preparation of Ultrathin SnO_2 Nanorods. In a typical synthesis, 0.1 g of $SnCl_4 \cdot 5H_2O$, 1 g of $CO(NH_2)_2$, and 2 mL of fuming HCl were added to 40 mL of superpure water under mild stirring, forming a colorless transparent aqueous solution. This solution was transferred into a Teflon-lined stainless steel autoclave of 50-mL capacity. The autoclave was sealed and maintained at 90 °C for 24 h. Finally, the autoclave was cooled down to room temperature naturally. The resulting white product was retrieved by centrifugation and washed several times with superpure water and absolute ethanol, and then dried in vacuum at 50 °C for 4 h.

Characterization. X-ray diffraction (XRD) patterns of the products were recorded on a Rigaku (Japan) D/max-γA X-ray diffractometer equipped with graphite monochromatized Cu−Kα radiation (λ = 1.54178 Å). Samples for transmission electron microscopy (TEM) analysis were prepared by drying a drop of nanocrystal dispersion in absolute ethanol on amorphous carbon-coated copper grids. Particle sizes and shapes high-resolution TEM (HRTEM) characterization was performed with a JEOL 2010 operated at 200 kV. The Raman spectrum was produced at room temperature on a Spex 1403 Raman spectrometer with an argon-ion laser at an excitation wavelength of 514.5 nm. UV−vis absorption spectra were recorded with a Shimadzu UV-2500. Photoluminescence (PL) measurements were carried out by using a Perkin-Elmer LS-55 luminescence spectrometer with a pulsed Xe lamp.

Gas-Sensing Measurement. The SnO_2 sensor was fabricated by dip-coating as-prepared SnO_2 alcohol colloids to the ceramic tube of the sensor body without an additional annealing process except for aging in the gas sensor system. The sensitivity (S) is defined as $S = R_a/R_g$, where R_a is the resistance in atmospheric air (its relative humidity is about 25%) and R_g is the resistance of the SnO_2 nanorods in ethanol-air mixed gas. R_a is around 4.7 MΩ in atmospheric air at the working temperature of 270 °C.

Water Treatment Experiment. Ten milligrams of the absorbent was added into 25 mL of acid fuchsine aqueous solution (1.0×10^{-4} M) in a flask reactor (capacity ca. 100 mL) at room temperature. The suspension was stirred magnetically in the dark. UV−vis absorption spectra were recorded at different intervals to monitor the absorption process using a Shimadzu-2550 spectrophotometer.

Results and Discussion

Morphology and Structure. The structure and morphology of these SnO_2 nanorods were investigated by TEM. Figure 1a shows the overall morphology of the sample, which indicates that the obtained product consists of large quantities of rod-like structures. The enlarged TEM image shown in Figure 1b reveals that these small nanorods are 2.0 ± 0.5 nm in diameter and 12 ± 3 nm in length. The bright ring patterns from selected area electron diffraction (SAED) given in Figure 1c can be well indexed to the rutile phase structure of SnO_2. The HRTEM image, Figure 1d, demonstrates the single-crystal nature of the SnO_2 nanorods. The lattice spacing of 0.318 nm between adjacent lattice planes in the image corresponds to the distance between two (001) crystal planes, confirming [001] as the preferred growth direction for the rutile phased SnO_2 nanorods. Energy dispersive

(12) Wang, G.; Lu, W.; Li, J. H.; Choi, J.; Jeong, Y.; Choi, S. Y.; Park, J. B.; Ryu, M. K.; Lee, K. *Small* **2006**, *2*, 1436.
(13) Xu, X.; Zhuang, J.; Wang, X. *J. Am. Chem. Soc.* **2008**, *130*, 12527.
(14) (a) Chowdhuri, A.; Gupta, V.; Sreenivas, K.; Kumar, R.; Mozumdar, S.; Patanjali, P. K. *Appl. Phys. Lett.* **2004**, *84*, 1180. (b) Liu, Koep, Y. E.; Liu, M. *Chem. Mater.* **2005**, *17*, 3997.
(15) Wang, Y. L.; Jiang, X. C.; Xia, Y. N. *J. Am. Chem. Soc.* **2003**, *125*, 16176.
(16) (a) Zhang, D. F.; Sun, L. D.; Yin, J. L.; Yan, C. H. *Adv. Mater.* **2003**, *15*, 1022. (b) Zhang, D. F.; Sun, L. D.; Xu, G.; Yan, C. H. *Phys. Chem. Chem. Phys.* **2006**, *8*, 4874.
(17) Kolmakov, A.; Zhang, Y.; Cheng, G.; Moskovits, M. *Adv. Mater.* **2003**, *15*, 997.
(18) Chen, D. L.; Gao, L. *Chem. Phys. Lett.* **2004**, *398*, 201.
(19) Cheng, B.; Russell, J. M.; Shi, W. S.; Zhang, L.; Samulski, E. T. *J. Am. Chem. Soc.* **2004**, *126*, 5972.

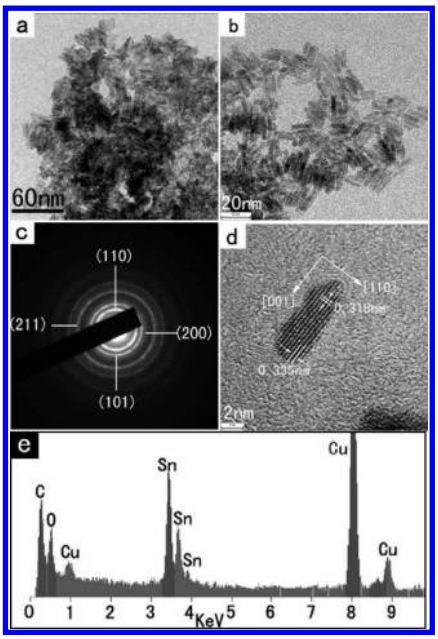

Figure 1. (a) Low-magnification TEM image of the SnO_2 nanorods. (b) High-magnification TEM image of the SnO_2 nanorods. (c) SAED pattern of the SnO_2 nanorods. (d) HRTEM image of a single SnO_2 nanorod. (e) EDS spectrum of the ultrathin SnO_2 nanorods.

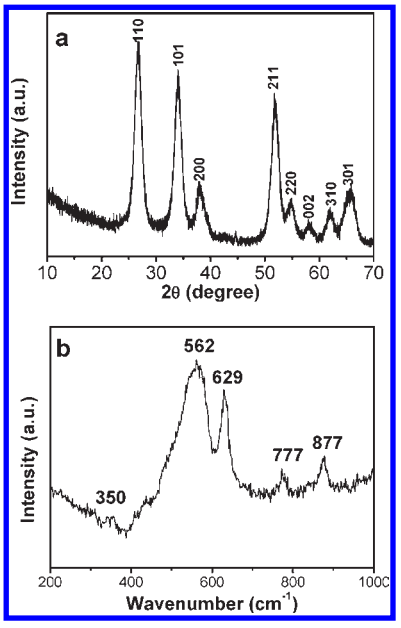

Figure 2. (a) Typical XRD pattern of the as-synthesized ultrathin SnO_2 nanorods. (b) A typical Raman spectrum of the ultrathin SnO_2 nanorods.

X-ray spectroscopy (EDS) characterizations demonstrated that the rod-like structures are composed of tin and oxide (Figure 1e). Tin and oxide peaks can be clearly observed in this spectrum. The Cu and C peaks in the EDS spectrum arise from the copper TEM grid used in the measurements.

The powder XRD pattern of the as-synthesized SnO_2 nanorods sample is shown in Figure 2a. The diffraction peaks reveals that the SnO_2 nanorods have a tetragonal crystal structure with lattice parameters $a = b = 4.74$ Å and $c = 3.19$ Å, which are well matched with those of the corresponding bulk rutile SnO_2 ($P4_2/mnm$, $a = b = 4.7382$ Å and $c = 3.1871$ Å, JPCDS No. 41−1445), while peaks are obviously broadened with decreasing crystal size. No other crystalline impurities were detected in the synthesized product. The Brunauer−Emmett−Teller (BET) result indicates that the specific area of the ultrathin SnO_2 nanorods is 191.5 $m^2\ g^{-1}$. Consequently, from the results of the XRD, EDS, and BET analyses, the as-synthesized product could be determined to be pure rutile phase SnO_2 with high specific area.

Raman scattering is a useful tool for the characterization of nanosized materials and a qualitative probe of the presence of lattice defects in solids.[20] At the same time, Raman spectroscopy is sensitive to crystal surface area.[21] The Raman spectrum of as-synthesized sample shows the presence of five peaks at 350, 562, 629, 777, and 877 cm^{-1} (Figure 2b). Among the peaks, Raman peaks at 629 and 777 cm^{-1} can be indexed to A_{1g} and B_{2g} vibration modes, respectively.[22] However, the Raman peaks at 350, 562, and 877 cm^{-1} are not detected in the bulk rutile SnO_2. In addition, compared with the Raman peaks of bulk rutile SnO_2, the Raman peaks of the present SnO_2 nanorods are considerably broader. Fauchet et al. and Richter et al. reported that while Si nanocrystals are smaller than 30 nm, it would lead to down shift and broadening of the Raman spectrum.[23,24] Chuu et al. found that for small CdS crystallites with diameters ranging from 3 to 100 nm the size effect is manifested by addition to the normal modes of the single crystal.[25] Therefore, these new Raman modes, being related to the facet surface area of a crystal, arise from nanoscaled SnO_2 with small grain size. This finding agrees very well with the Matossi force constant model.[26] The Raman spectrum confirms the characteristics of the tetragonal rutile structure as well as the very small size of the SnO_2 nanorods.

Optical Properties. High-energy shift of an absorption edge is generally expected for nanomaterials. To confirm this, the absorption spectrum was acquired from the ultrathin SnO_2 nanorods, and the results are shown in Figure 3a. The optical transition of SnO_2 crystals is known to be a direct type.[27] In this case, the absorption coefficient α is expressed as $\alpha(h\nu) \sim (h\nu - E_g)^{1/2}/h\nu$.[28] Plots of $(\alpha(h\nu))^2$ versus $h\nu$ can be derived from the absorption data in Figure 3a. The intercept of the tangent to the plot gives a good approximation of the band gap energy of the direct band gap materials. This is ~4.72 eV for the ultrathin nanorods, as shown in the inset of Figure 3a, which are far larger than the value of 3.62 eV for bulk SnO_2 because of the strong quantum size effect.

Figure 3b shows the room-temperature photoluminescence spectra of the ultrathin SnO_2 nanorods, which were measured by using a Perkin−Elmer LS-55 luminescence spectrometer with an excitation-slit width of 5 nm and an emission-slit width of 5 nm. A green emission centered at

(20) Torchynska, T. V.; Hernandez, A. V.; Cano, A. D.; Sandoval, S. J.; Ostapenko, S.; Mynbaeva, M. *J. Appl. Phys.* **2005**, *97*, 33507.
(21) Sun, S. H.; Meng, G. W.; Zhang, G. X.; Gao, T.; Geng, B. Y.; Zhang, L. D.; Zuo, J. *Chem. Phys. Lett.* **2003**, *376*, 103.
(22) Peercy, P. S.; Morosin, B. *Phys. Rev. B* **1973**, *7*, 2779.
(23) Campbell, I. H.; Fauchet, P. M. *Solid State Commun.* **1986**, *58*, 739.
(24) Richter, H.; Wang, P. M.; Ley, L. *Solid State Commun.* **1981**, *39*, 625.
(25) Chuu, D. S.; Dai, C. M.; Hsieh, W. F.; Tsai, C. T. *J. Appl. Phys.* **1991**, *69*, 8402.
(26) Zuo, J.; Xu, C.; Liu, X.; Wang, C.; Wang, C.; Hu, Y.; Qian, Y. *J. Appl. Phys.* **1994**, *75*, 1835.
(27) Frohlich, D.; Kenklies, R. *Phys. Rev. Lett.* **1978**, *41*, 1750.
(28) Mills, G.; Li, Z. G.; Meisel, D. *J. Phys. Chem. B* **1988**, *92*, 822.

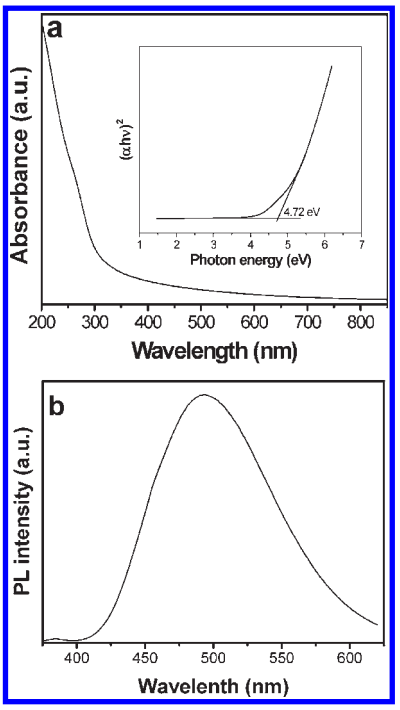

Figure 3. (a) UV−vis adsorption of the as-synthesized ultrathin SnO_2 nanorods. (b) A typical room-temperature photoluminescence spectrum of the ultrathin SnO_2 nanorods.

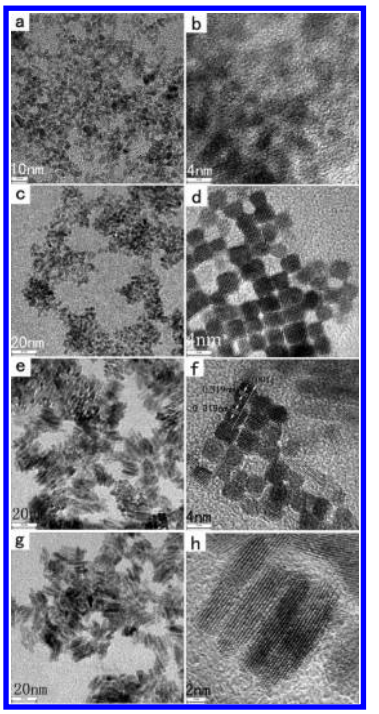

Figure 4. TEM and HRTEM images of the products prepared at 90 °C for various time: (a, b) 3 h, (c, d) 8 h, (e, f) 15 h, and (g, h) 24 h.

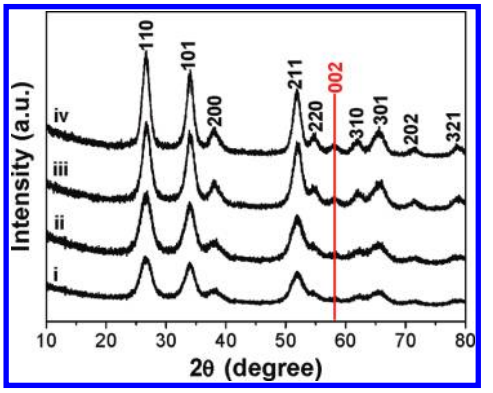

Figure 5. XRD patterns of SnO2 samples prepared at 90 °C for (i) 3 h, (ii) 8 h, (iii) 15 h, and (iv) 24 h.

493 nm (2.51 eV) was observed from the ultrathin SnO_2 nanorods. Since the band gap of the present SnO_2 nanorods is 4.72 eV as determined from the UV/visible absorption spectrum, the observed green luminescence band cannot be ascribed to the direct recombination of a conduction electron in the Sn 4d band with a hole in the O 2p valence band. The nature of the transition is generally believed to be Sn or O vacancies formed during the growth process inducing trapping states in the band gap. A similar emission has been reported in the case of SnO_2 polycrystalline nanowires synthesized by the solvothermal route.[13]

Morphology Evolution Process and Growth Mechanism. To investigate the growth process of the ultrathin nanorods, a series of experiments were carried out, as discussed below. We followed the nucleation and growth steps by studying the samples obtained at different reaction stages using the TEM, HRTEM, and XRD techniques. Figure 4a−h shows the TEM and HRTEM images of the samples obtained after the reaction performed for 3 h, 8 h, 15 h, and 24 h, respectively. These images distinctly reveal the transformation process of the particle morphology from the nanoparticles to nearly monodisperse nanocubes, to short nanochains, and finally to single-crystalline nanorods.

Figure 4a,b shows the TEM and HRTEM images of the product obtained after 3 h, indicating the product consisted of sphere-like SnO_2 nanoparticles about 1−1.5 nm in diameter. If the reaction time was prolonged to 8 h, most of the SnO_2 nanoparticles were developed into single-crystalline cube-like nanocrystals (Figure 4c,d). The cubes were about 2 nm in width. It should be noted that the size of the cubes is consistent with the diameter of the final SnO_2 nanorods. After 15 h reaction, most of the nanocubes in the solution spontaneously reorganized into short nanochains (Figure 4e,f). The HRTEM image indicates that the SnO_2 nanocubes contained in one nanochain are bound to each other on (001) faces, leading to the particle attachment along the [001] direction, which is consisted with the growth direction of the final nanorods. Finally, as the reaction time increased enough (24 h), single-crystalline SnO_2 nanorods were formed by the recrystallization of multiple nanocubes contained in a chain-like aggregate that fused gradually into one crystal (Figure 4g-h).

Time-dependent XRD patterns (Figure 5) reveal the crystallographic orientation transformation from nanoparticles to nanorods. For the initial nanoparticles and nanocubes, no obvious (002) diffraction peak was detected. For the intermediate nanochains, a detectable (002) diffraction peak can be seen. For the single-crystalline nanorods, the (002) diffraction peak is stronger. The enhancement of the (002) diffraction peak can be attributed to the oriented attachment of SnO_2 nanocubes by binding to each other on (001) faces, which is consistent with the observation of TEM and HRTEM.

From the above experimental observations, we believe that formation of the ultrathin SnO_2 nanorods can be rationally expressed as a kinetically controlled nonclassical crystallization process: classical Ostwald ripening process followed by a nonclassical oriented attachment mechanism. First, when the hydrolysis reaction was carried out in the solution system at 90 °C for 3 h, it generated rutile phase SnO_2 small nanoparticles, which were formed in the solution through a homogeneous nucleation process. Then, to minimize the overall energy of the system, the small SnO_2 nanoparticles started to dissolve into the solution and grow onto large nanoparticles of SnO_2 via a classical crystallization process known as Ostwald ripening. Because of the ripening mechanism, the large nanoparticles gradually evolved into nanocubes. Subsequently, the nanocubes assembled into short nanochains by binding to each other on (001) faces. Finally, the linear aggregates recrystallized into single-crystalline nanorods whose diameter was determined by the diameter of the nanocubes. Therefore, the present SnO_2 nanorods are prepared through the synergic effect of ripening mechanism and oriented attachment. A classical Ostwald ripening process generated the intermediate nanocubes; subsequently, a nonclassical particle-based crystallization process yields the single-crystalline nanorods. In summary, the chemical reactions contained in the formation procedure of the SnO_2 nanorods can be seen in eqs 1, 2, and 3:

$$CO(NH_2)_2 + H_2O \rightarrow CO_2 + 2NH_3 \quad (1)$$

$$NH_3 + H_2O \rightleftarrows NH_4^+ + OH^- \quad (2)$$

$$Sn^{4+} + 4OH^- \rightarrow Sn(OH)_4 \rightarrow SnO_2 + 2H_2O \quad (3)$$

Then, what is the driving force for the oriented attachment of the SnO_2 nanocubes? The growth of nanorods or nanowires by oriented attachment of small nanocrystals has been reported for several materials, such as CdTe nanowires,[29] ZnO nanorods,[30] PbSe nanowires and nanorings,[31] ZnS nanorods,[32] and CdSe nanowires,[33] Cu nanowires,[34] and In_2O_3 nanowires.[35] The driving forces of the 1-D oriented attachment of nanocrystals were generally attributed to the dipole−dipole interactions induced by the inherent anisotropy of crystal structure, interactions between organic long-chain molecules, and weak interaction between magic-sized clusters. However, it seems that these driving forces mentioned-above cannot be fully used to explain the formation of the present ultrathin SnO_2 nanorods because of the following: (1) no polar surfaces along the [001] direction of rutile phase SnO_2;[11c] (2) no long-chain organic molecules were used in the present reaction; (3) as the primary built unit of the self-assembled nanochains, the size of the nanocubes is far larger than that of magic-sized clusters. For rutile phase SnO_2, computer simulation studies have demonstrated that the sequence of surface energy in different crystallographic orientations is (001) > (101) > (100) > (110), that is, the (001) crystal face has the highest surface energy.[36−38] Therefore, according to the Lowest Energy principle, the [001] direction theoretically is a preferential growth direction of the SnO_2 nanocrystals. Here, HRTEM image (Figure 4f) clearly demonstrated that the SnO_2 nanocubes bind to each other on (001) faces to maximally reduce their surface energies, which offer a convincing evidence to support that surface energy probably is a driving force in the oriented attachment process of SnO_2 nanocubes. The formation process of the nanorods is summarized in Figure 6.

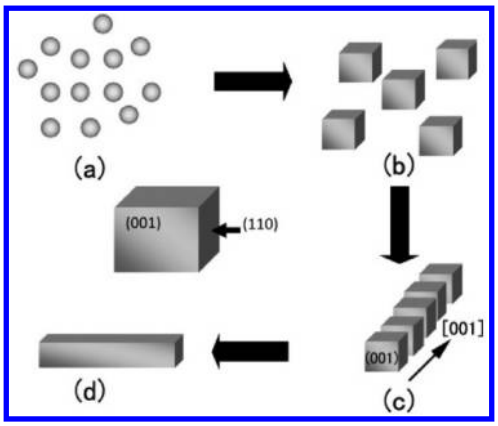

Figure 6. Schematic illustration of the formation and shape evolution of the ultrathin SnO_2 nanorods: (a) Formation of sphere-like SnO_2 nanoparticles after 3 h reaction; (b) Formation of nanocubes by a Ostwald ripening process; (c) Formation of SnO_2 nanochains through SnO_2 nanocubes bind to each other on (001) faces; (d) SnO_2 nanochains grown into single-crystalline nanorods by fusion and recrystallinity of SnO_2 nanocubes.

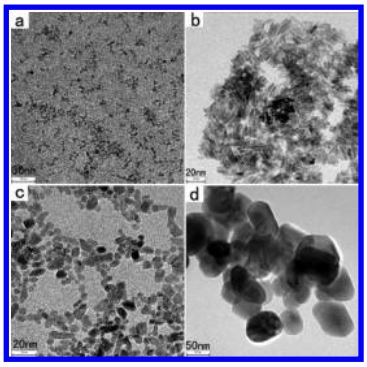

Figure 7. TEM images of the SnO_2 nanocrystals prepared in different urea concentration: (a) 0.2 g, (b) 0.6 g, (c) 2 g, and (d) 4 g. In all case, the reaction was carried out at 90 °C for 24 h.

Influencing Factors. Controlled experiments indicate that the concentration of the urea solution is crucial for the formation of the ultrathin SnO_2 nanorods. Figure 7 exhibits the morphologies of the products obtained from

(29) Tang, Z. Y.; Kotov, N. A.; Giersig, M. *Science* **2002**, *297*, 237.
(30) Pacholski, C.; Kornowski, A.; Weller, H. *Angew. Chem., Int. Ed.* **2002**, *41*, 1188.
(31) Cho, K. S.; Talapin, D. V.; Gaschler, W.; Murray, C. B. *J. Am. Chem. Soc.* **2005**, *127*, 7140.
(32) Yu, J. H.; Joo, J.; Park, H. M.; Baik, S. I.; Kim, Y. W.; Kim, S. C.; Hyeon, T. *J. Am. Chem. Soc.* **2005**, *127*, 5662.
(33) Pradhan, N.; Xu, H. F.; Peng, X. G. *Nano Lett.* **2006**, *6*, 720.
(34) Shen, S. L.; Zhuang, J.; Xu, X. X.; Nisar, A.; Hu, S.; Wang, X. *Inorg. Chem.* **2009**, *48*, 5117.
(35) Xu, X. X.; Wang, X. *Inorg. Chem.* **2009**, *48*, 3890.
(36) Slater, B.; Catlow, C. R. A.; Gay, D. H.; Williams, D. E.; Dusastre, V. *J. Phys. Chem. B.* **1999**, *103*, 10644.
(37) Leite, E. R.; Giraldi, T. R.; Pontes, F. M.; Longo, E.; Beltran, A.; Andres, J. *Appl. Phys. Lett.* **2003**, *83*, 1566.
(38) Oviedo, J.; Gillan, M. J. *Surf. Sci.* **2000**, *463*, 93.

the aqueous solution of urea with different concentration when keeping other experimental conditions unchanged. In the absence of urea, no crystalline products were obtained. When 0.2 g of urea was added into the reaction mixtures, the products consist of lots of nanoparticles with very small sizes (Figure 7a). When the amount of urea is increased to 0.6 g, the product is a mixture of nanorods and nanoparticles (Figure 7b). When the amount of urea is increased to 2 g, ~10 nm sized SnO_2 nanoparticles were obtained (Figure 7c). When the amount of urea is further increased to 4 g, ~50 nm sized SnO_2 nanoparticles were obtained (Figure 7d). These results indicate that ultrathin SnO_2 nanorods can only be synthesized in a solution that contains a suitable amount of urea. As a hydrolysis agent, the concentration of urea may control the hydrolysis rate of Sn^{4+}. When reaction occurs at a low concentration of urea, the concentration of NH_3 generated by the hydrolysis of urea is low (reaction eq 1). As a result, the concentration of OH^- generated from the hydrolysis of NH_3 is low (reaction eq 2). The low concentration of OH^- restrains the hydrolysis of the Sn^{4+} (reaction eq 3). Therefore, the nucleation rate of SnO_2 is much faster than the rate of crystal growth because of the existence of a small quantity of $Sn(OH)_4$ (reaction eq 3). Large quantities of SnO_2 nuclei tend to orient and aggregate together to form larger and more thermodynamically stable nanorods. On the contrary, when the concentration of urea is high, the concentration of Sn^{4+} ions is greatly reduced because of the hydrolysis of the Sn^{4+}; therefore, the rate of SnO_2 nucleation is then depressed, which slows down the aggregation of SnO_2 nuclei before the crystal growth of SnO_2 during the solution-phase process. Large SnO_2 nanoparticles are formed under these conditions instead of nanorods.

We further investigated the effect of reaction temperature on the morphology of the SnO_2 nanostructures. The sample prepared at 120 °C for 24 h was composed of nanorods and nanocrystals (Figure 8a). The diameter of the nanorods is about 4−5 nm. When the hydrolysis reaction was performed at 140 °C, the obtained products are nanorods with an average diameter of 15 nm (Figure 8b, sample A). When the reaction temperature was increased to 160 °C, the obtained products are composed of a large number of uniform SnO_2 nanowires (Figure 8c, sample B). The nanowires are about 30 nm in diameter and several micrometers in length. When the reaction temperature was further increased to 200 °C, the products are uniform nanorods, which are about 40 nm in diameter and 600 nm in length (Figure 8d, sample C). These controlled experimental observations suggest that a more rapid hydrolysis at higher temperature favors the formation of relative larger 1-D SnO_2 nanostructures, suppressing the growth of ultrathin nanorods.

Gas-Sensing Properties. Since the as-synthesized ultrathin SnO_2 nanorods have high crystallinity, large surface area, it can be expected that the SnO_2 nanorods possess an enhanced gas-sensing performance. To test this, we investigated the C_2H_5OH gas sensing properties of the as-synthesized SnO_2 nanorods. The sensitivity (S) is defined as $S = R_a/R_g$, where R_a is the resistance in atmospheric air (its relative humidity is about 25%) and R_g is the resistance of the SnO_2 nanorods in ethanol-air mixed gas. R_a is around 4.7 MΩ in atmospheric air at the working

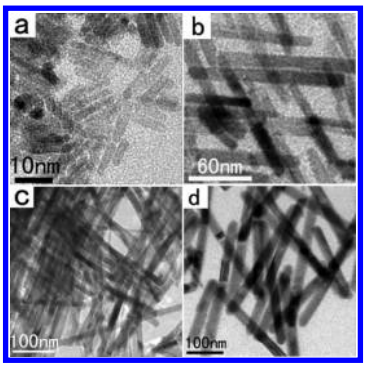

Figure 8. TEM images of the SnO_2 nanocrystals prepared at different reaction temperature for 24 h: (a) 120 °C, (b) 140 °C, (c) 160 °C, and (d) 200 °C.

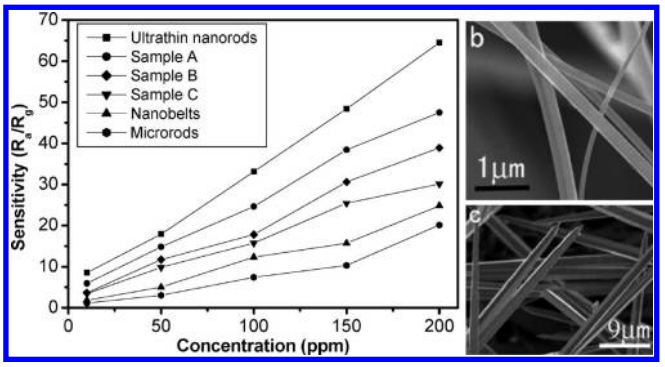

Figure 9. (a) Relationship between the sensor sensitivity and the ethanol concentration of the samples. (c) The SEM image of the SnO_2 microrods. The preparation of SnO_2 nanobelts and microrods is based on the thermal evaporation route described by Hu et al.[45].

temperature of 270 °C. The experimental results demonstrated that the ultrathin SnO_2 nanorod has a very high sensitivity to ethanol, as shown in Figure 9. The sensitivities of the ultrathin SnO_2 nanorods are 8.5, 17.9, 33.1, 48.4, and 64.5 to 10, 50, 100, 150, and 200 ppm ethanol vapor, respectively. As comparison, sample A, sample B, sample C, SnO_2 nanobelts, and microrods were selected to evaluate the ethanol gas-sensing performance, respectively. Keeping the experimental parameters unchanged, it was found that the as-synthesized ultrathin SnO_2 nanorods have obviously better gas-sensing properties than those of the sample A, sample B, sample C, SnO_2 nanobelts, and microrods. Furthermore, compared with the ethanol gas-sensing properties of SnO_2 nanorods (31.4 to 300 ppm),[39] hollow spheres (7.5 to 50 ppm),[40] and nanotubes (8 to 20 ppm),[41] reported by others, those of the as-synthesized ultrathin SnO_2 nanorods are superior.

As for the sensing mechanism of ultrathin SnO_2 nanorods, it involves the interaction between ethanol and the chemisorbed oxygen ions on the surface of the ultrathin SnO_2 nanorods, such as O_2^-, O^-, and O^{2-}.[42] It is well-known that a space-charge-layer (SCL) will form on the surface of the SnO_2 when an electron from semiconducting SnO_2 is trapped by adsorbed oxygen species. Because

(39) Chen, Y. J.; Xue, X. Y.; Wang, Y. G.; Wang, T. H. *Appl. Phys. Lett.* **2005**, *87*, 233503.
(40) Zhao, Q. R.; Gao, Y.; Bai, X.; Wu, C. Z.; Xie, Y. *Eur. J. Inorg. Chem.* **2006**, 1643.
(41) Huang, J.; Matsunaga, N.; Shimanoe, K.; Yamazoe, N.; Kunitake, T. *Chem. Mater.* **2005**, *17*, 3513.
(42) Chiu, H. C.; Yeh, C. S. *J. Phys. Chem. C* **2007**, *111*, 7256.

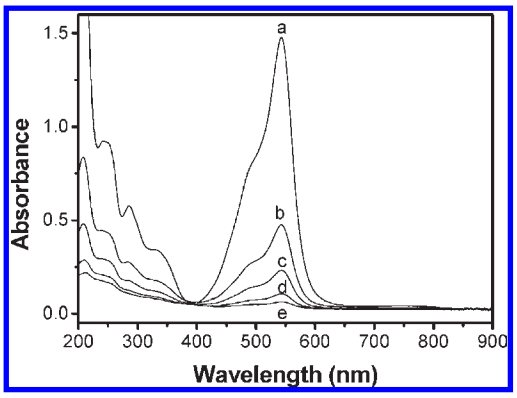

Figure 10. Absorption spectra of a solution of acid fuchsine (1.0×10^{-4} M, 25 mL) in the presence of ultrathin SnO_2 nanorods (10 mg) at different time intervals of (a) 0 min; (b) 2 min; (c) 5 min; (d) 10 min; and (e) 20 min, respectively.

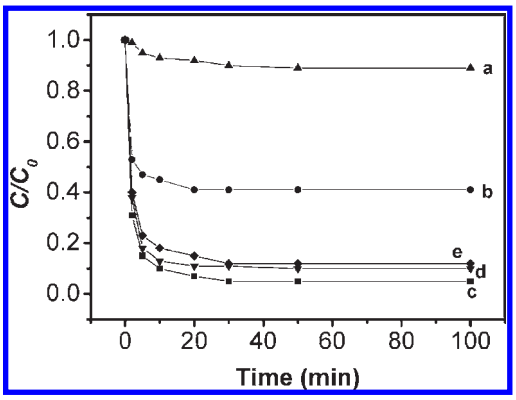

Figure 11. Adsorption rate of the azo-dye acid fuchsine on (a) commercial SnO_2; (b) commercial TiO_2; (c) fresh ultrathin SnO_2 nanorods; (d) secondary; and (e) third, respectively.

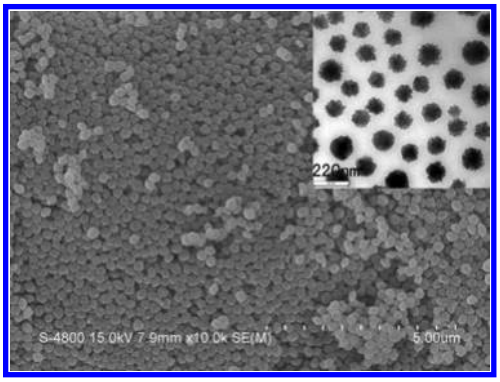

Figure 12. FESEM and TEM (insert) images of the self-assembled SnO_2 submicrometer spheres from the ultrathin nanorods.

the ethanol reacts with the ionic oxygen species, the electrons trapped by the oxygen adsorbents are released to the metal oxides. As a result, the conductivity of the SnO_2 will increase. Earlier studies demonstrated that the SnO_2 nanostructure will exhibit better gas-sensing properties when its size is reduced to a scale close to or smaller than the double of SCL thickness (for SnO_2, its SCL thickness is 3 nm).[43] In the present work, the diameters of the ultrathin SnO_2 nanorods are only 2 ± 0.5 nm, which is obviously smaller than the SCL thickness of SnO_2. Therefore, as a result, the as-synthesized ultrathin SnO_2 nanorods display a very high sensitivity to ethanol gas. In addition, we believe that the higher sensitivity of the ultrathin SnO_2 nanorods might be attributed to their single-crystalline structure, which make the electron transfer become easy in the SCL. Furthermore, the sensitivity of the ultrathin SnO_2 nanorods is directly proportional to the concentration of ethanol gas. The linear relation between sensitivity and gas concentration can be expressed as $S = A[C]^N$, where A is a constant, and C is the gas concentration. The value of N is 1 or 1/2. Generally, the value of N is 1 when the size of the SnO_2 nanoparticles is comparable with the SCL thickness of SnO_2, while the value is 1/2 when the size of the SnO_2 nanoparticles increases to more than 20 nm.[39,44] Since the diameter of the nanorods is only 2 ± 0.5 nm, the value of N is 1. Here, such a linear dependence of the sensitivity on the ethanol concentration further suggests that the ultrathin SnO_2 nanorods can be used as a promising material for the fabrication of gas sensors.

Applications in Water Treatment. We further used the as-obtained SnO_2 nanorods to investigate their applications in water treatment. Acid fuchsine, a common azo-dye in the textile industry, was chosen as a typical organic waste and was the characteristic absorption of acid fuchsine at about 545 nm for monitoring the adsorption process. Figure 10 indicates the absorption spectra of an aqueous solution of acid fuchsine (initial concentration: 1.0×10^{-4} M, 25 mL) in the presence of 10 mg of as-synthesized ultrathin SnO_2 nanorods under stirring in the dark. As shown in Figure 10, the absorbance intensity of the peak corresponding to the acid fuchsine molecule at 545 nm decreased very quickly once SnO_2 nanorods were added. With time increasing, the typical sharp peak at 545 nm almost completely vanished after 20 min. As comparison, the commercial SnO_2 and TiO_2 nanoparticles were selected to evaluate the absorb capacity of acid fuchsine, respectively. Keeping the experimental parameters unchanged, it was found that the as-synthesized ultrathin SnO_2 nanorods have obviously better removal ability than the commercial SnO_2 and TiO_2 (Figure 11a−c). This might be attributed to the very small diameter and high surface area of the as-synthesized SnO_2 nanorods. Interestingly, it was found that sphere-like aggregations would form once the SnO_2 nanorods adsorb acid fuchsine (Figure 12). These spheres have relative larger diameters (about 200 nm); therefore, they can be conveniently separated from the solution, which is of considerable importance in the practical water treatment applications. In addition, the SnO_2 submicrospheres containing acid fuchsine could be renewed by annealing at 270 °C in air for 5 h, and the renewed SnO_2 materials held almost the same adsorption capability as shown in Figure 11d,e. These results indicate the promising potential of using the as-obtained SnO_2 materials as efficient water treatment material for environment cleaning.

Conclusion

In summary, we have demonstrated the synthesis of ultrathin SnO_2 single-crystalline nanorods via a simple hydrolysis

(43) Ogawa, H.; Nishikawa, M.; Abe, A. *J. Appl. Phys.* **1982**, *53*, 4448.
(44) Wan, Q.; Li, Q. H.; Chen, Y. J.; Wang, T. H.; He, X. L.; Li, J. P.; Lin, C. L. *Appl. Phys. Lett.* **2004**, *84*, 3654.
(45) Hu, J. Q.; Ma, X. L.; Shang, N. G.; Xie, Z. Y.; Wong, N. B.; Lee, C. S.; Lee, S. T. *J. Phys. Chem. B* **2002**, *106*, 3823.

reaction of tin tetrachloride with urea at 90 °C, without using any template and surfactant. The present synthetic route has a few advantages, such as low temperature, green-friendly, and low cost. Ultrathin SnO_2 single-crystalline nanorods are obtained through the synergic effect of Ostwald ripening mechanism and oriented attachment process. Surface energy was found as a possible driving force for the self-assembly of SnO_2 nanocrystals, which allow us to further research the oriented attachment mechanism. The shape evolution of nanocrystals in the present reaction system should be valuable for the precise understanding of the ultrathin nanowire structures. The as-synthesized ultrathin rod-like structure endows the SnO_2 with superior gas-sensing activity. Meanwhile, the as-synthesized SnO_2 quantum rods showed an excellent ability to remove an organic pollutant in wastewater.

Acknowledgment. This work was in part supported by World Premier International Research Center Initiative (WPI Initiative) on Materials Nanoarchitectonics, the Global Environment Research Fund, MEXT, Japan and the Strategic International Cooperative Program, Japan Science and Technology Agency (JST).